BNL-103698-2014-TECH

AGS/RHIC/SN 073;BNL-103698-2014-IR

Data Reduction of Field Measurement by the Hall Probe for Half-Length Helical Dipole Prototype

T. Tominaka

June 1998

Collider Accelerator Department

Brookhaven National Laboratory

U.S. Department of Energy

USDOE Office of Science (SC)

DISCLAIMER

Alternating Gradient Synchrotron Department
Relativistic Heavy Ion Collider Project
BROOKHAVEN NATIONAL LABORATORY
Upton, New York 11973

Spin Note

AGS/RHIC/SN No. 073

Data Reduction of Field Measurement by the Hall Probe for Half-Length Helical Dipole Prototype

T. Tominaka
RIKEN

June 10, 1998

Data Reduction of Field Measurement by the Hall Probe for Half-Length Helical Dipole Prototype

T. Tominaka (RIKEN, Japan)

June 3, 1998

1 INTRODUCTION

Comparison between the field measurement by the Hall probe and 3D field calculation with TOSCA for the half-length helical dipole prototype is presented with the emphasis on the relation among the phase angles of helical multipoles.

2 DATA REDUCTION OF MAGNETIC FIELD OF HELICAL DIPOLE

2.1 Methods of Data Analysis

On this data analysis, the data measured by the Hall probe located at the large radius (r = 35.6 mm) is only used, differently from the previous reports.[2,3,4] This seems to be reasonable from the fact that the accuracy of the data measured by the Hall probe located at the large radius is much higher than those at the small radius (r = 6.6 mm). It can be considered that the phase angles of the higher multipoles like sextupole, decapole, etc., rotate along the beam axis similarly with that of the dipole, in the helical body portion, because the cross-sectional configuration in the helical body portion of the helical dipole is same. These phase angles can be defined from the fundamental expressions for the magnetic field of helical dipoles. The interior magnetic field of helical dipole magnet with the infinite length can be expressed as follows, [5]

$$\begin{cases} B_r(r,\theta,z) = B_{ref}(k)\, r_0 \sum_{n=1}^{\infty} n! \left[\frac{2}{n\,k\,r_0}\right]^n k\, I_n'(n\,k\,r) \left\{-a_n(k)\cos\left(n(\theta - k\,z)\right) + b_n(k)\sin\left(n(\theta - k\,z)\right)\right\} \\ B_\theta(r,\theta,z) = B_{ref}(k)\, r_0 \sum_{n=1}^{\infty} n! \left[\frac{2}{n\,k\,r_0}\right]^n \frac{I_n(n\,k\,r)}{r} \left\{a_n(k)\sin\left(n(\theta - k\,z)\right) + b_n(k)\cos\left(n(\theta - k\,z)\right)\right\} \\ B_z(r,\theta,z) = B_{ref}(k)\, r_0 \sum_{n=1}^{\infty} (-k)\, n! \left[\frac{2}{n\,k\,r_0}\right]^n I_n(n\,k\,r) \left\{a_n(k)\sin\left(n(\theta - k\,z)\right) + b_n(k)\cos\left(n(\theta - k\,z)\right)\right\} \end{cases} \quad (1)$$

where $k = 2\pi/L$ is a twist pitch, and L is the length of the 2π rotation. In particular, the expressions for the radial field, B_r, and the tangential field, B_θ, with the allowed multipoles of helical dipoles can be rewritten into the following forms,

$$\begin{cases} B_r(r,\theta,z) = B_{r1}\sin\left[\theta - k\,z - \theta_{1,0}\right] + B_{r3}\sin\left[3\left(\theta - k\,z - \theta_{3,0}\right)\right] + B_{r5}\sin\left[5\left(\theta - k\,z - \theta_{5,0}\right)\right] + \cdots \\ \qquad = B_{r1}\sin\left[\theta - \theta_1(z)\right] + B_{r3}\sin\left[3\left(\theta - \theta_3(z)\right)\right] + B_{r5}\sin\left[5\left(\theta - \theta_5(z)\right)\right] + \cdots \\ B_\theta(r,\theta,z) = B_{\theta 1}\cos\left[\theta - k\,z - \theta_{1,0}\right] + B_{\theta 3}\cos\left[3\left(\theta - k\,z - \theta_{3,0}\right)\right] + B_{\theta 5}\cos\left[5\left(\theta - k\,z - \theta_{5,0}\right)\right] + \cdots \\ \qquad = B_{\theta 1}\cos\left[\theta - \theta_1(z)\right] + B_{\theta 3}\cos\left[3\left(\theta - \theta_3(z)\right)\right] + B_{\theta 5}\cos\left[5\left(\theta - \theta_5(z)\right)\right] + \cdots \end{cases} \quad (2)$$

As a result, the phase angle of 2n-pole, $\theta_n(z)$ can be defined as follows,

$$\theta_n(z) = k\,z + \theta_{n,0} \quad (3)$$

However, on the former analysis, the phase angle, $\theta'_n(z)$ was defined differently by the following equation,[2,3,4]

$$\theta'_n(z) = n\,\theta_n(z) = n\left(k\,z + \theta_{n,0}\right) \quad (4)$$

Then, the relation between the rotation of the phase angles of the higher multipole components and that of dipole component along the beam axis was not clear.

2.2 Comparison with 3D Field Calculation by TOSCA

The analyzed results for both of the data measured by the Hall probe at the large radius (r = 35.6 mm) and 3D field calculation by TOSCA are shown in Figs. 1 to 14 for two measurements at I = 105 A and 220 A. For the comparison at I = 105 A, the calculated results by TOSCA for I = 100 A is converted to that at I = 105 A with the multiplication of 1.05.[3] In addition, k = 2π/2.4 (rad/m) for the twist pitch of helical dipole, is used on the field calculation by TOSCA, neglecting the thermal contraction of Al coil bobbin (about 0.4 %).
From the analyzed results shown in Figs. 13 and 14, in the helical body portion, the following relation between the phase angles of the dipole and the higher multipole is obtained approximately, corresponding to the negative value of the normal sextupole component,

$$\begin{cases} \theta_3(z) = \theta_1(z) + \Delta\theta_3(z) \cong \theta_1(z) + 60° \\ \theta_5(z) = \theta_1(z) + \Delta\theta_5(z) \cong \theta_1(z) + 0° \end{cases} \quad (5)$$

On the comparison for the field intensity of 2n-poles, $B_{ref} \times (a_n^2+b_n^2)^{1/2}$ ($\approx B_{rn}(r_0)$ or $B_{\theta n}(r_0)$), in Eq. (1) with the reference radius of r_0 = 31 mm, derived from the measured radial field, B_r, at r = 35.6 mm and the calculated tangential field, B_θ, at r = 31 mm are plotted. Unfortunately, the measured field intensities of the sextupole and decapole include large errors, differently from the measurement by the rotating coil.

3 CONCLUSION

The definition for the phase angles of the helical multipoles in the helical dipoles is given consistently with the structure of the helical dipole. The field measurement with the Hall probe and the 3D calculation by TOSCA are compared on the basis of this definition. The improvements for the magnetic field measurement is thought to be necessary from some discrepancies between the magnetic field measurement and calculation.

4 ACKNOWLEDGMENT

The author is indebted for providing the experimental data to A. Jain, R. Thomas and E. Willen, and also for providing the calculated results of TOSCA and useful discussions to M. Okamura and T. Katayama.

REFERENCES

[1] R. Thomas, "Recalibration of Vertical Positions of Hall Probe Vertical Transporter", BNL Memorandum (1997).
[2] A. Jain, Private communications.
[3] M. Okamura, "The Hall Probe Measurement and Calculation of the Half Length Helical Dipole Magnet", AGS/RHIC/SN No.60, August 20, (1997).
[4] M. Okamura et al., "Field Calculations and Measurements of the Helical Snake Magnets for RHIC", Proc. of MT-15 (1997), Beijing, to be published.
[5] T. Tominaka et al., "Analytical Field Calculation of Helical Dipole Magnets for RHIC", Proc. of PAC (1997), Vancouver, to be published.

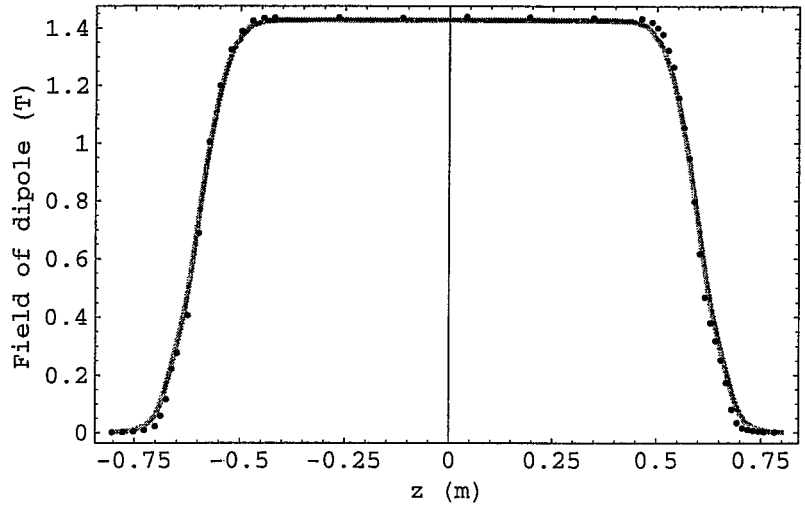

Fig.1. Comparison between measured (dots) and calculated (solid curve) filed intensities of dipole (n=1) along the beam axis at I = 105 A.

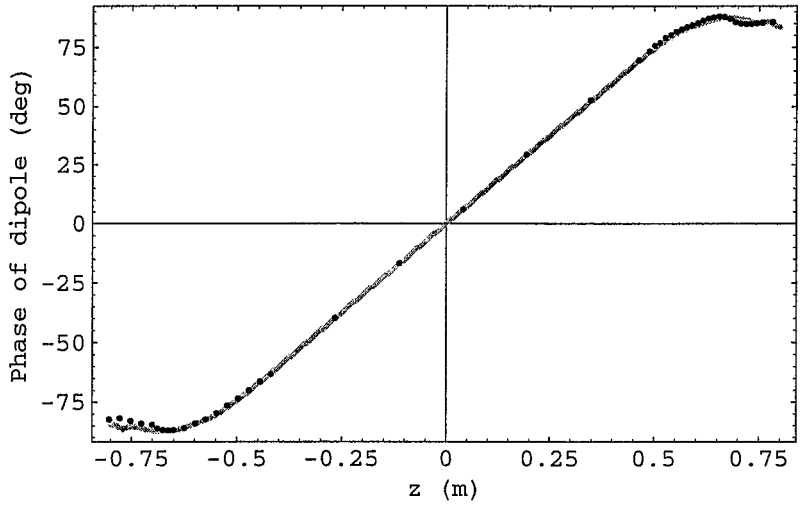

Fig.2. Comparison between measured (dots) and calculated (solid curve) phase angles of dipole (n=1) along the beam axis at I = 105 A.

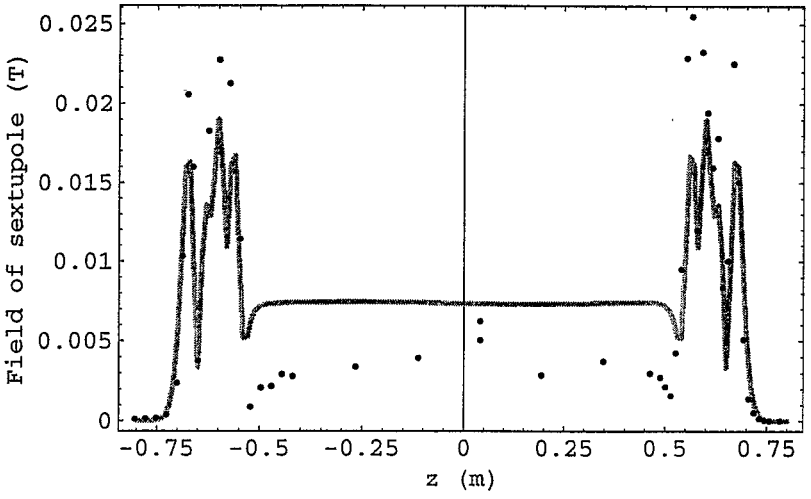

Fig.3. Comparison between measured (dots) and calculated (solid curve) filed intensities of sextupole (n=3) along the beam axis at I = 105 A.

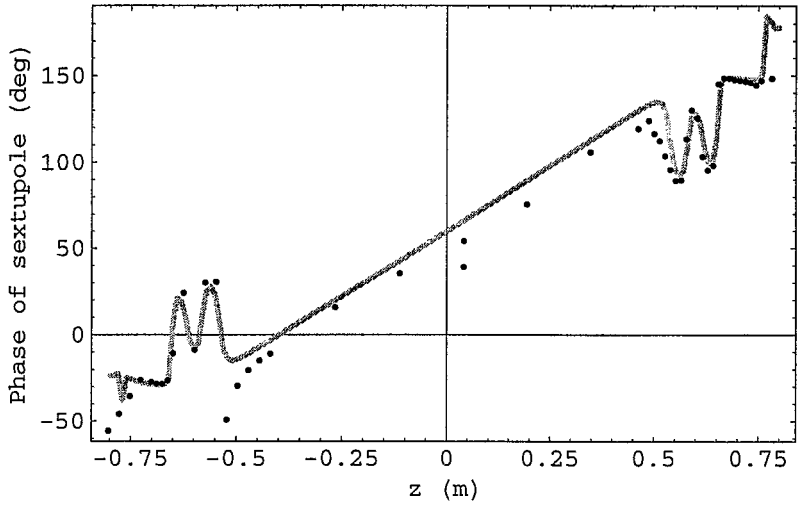

Fig.4. Comparison between measured (dots) and calculated (solid curve) phase angles of sextupole (n=3) along the beam axis at I = 105 A.

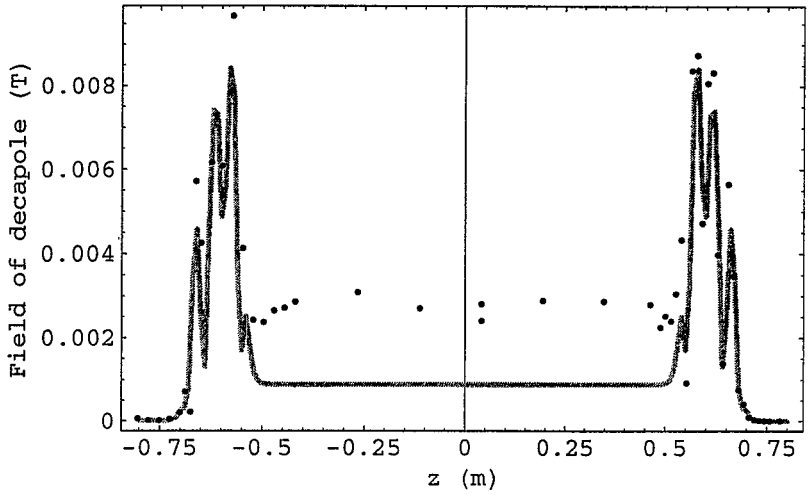

Fig.5. Comparison between measured (dots) and calculated (solid curve) filed intensities of decapole (n=5) along the beam axis at I = 105 A.

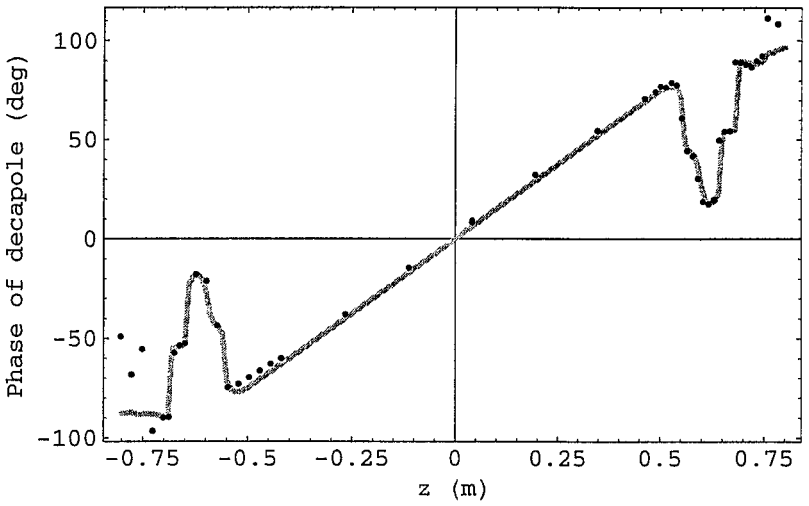

Fig.6. Comparison between measured (dots) and calculated (solid curve) phase angles of decapole (n=5) along the beam axis at I = 105 A.

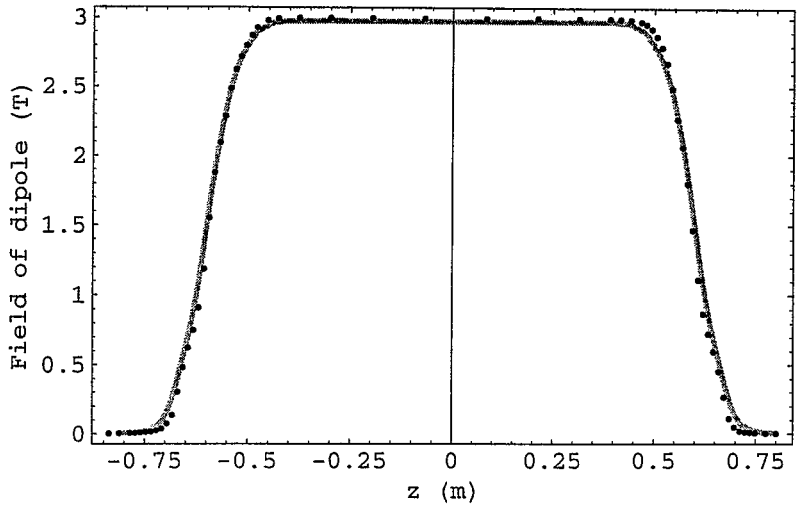

Fig.7. Comparison between measured (dots) and calculated (solid curve) filed intensities of dipole (n=1) along the beam axis at I = 220 A.

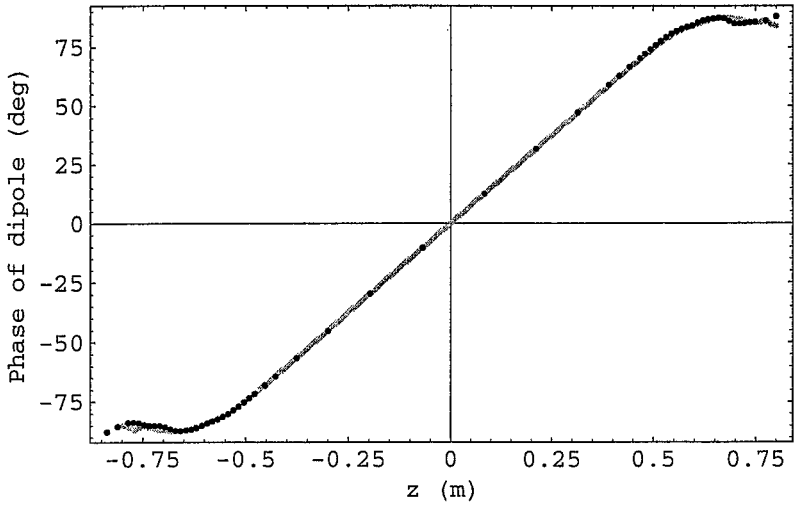

Fig.8. Comparison between measured (dots) and calculated (solid curve) phase angles of dipole (n=1) along the beam axis at I = 220 A.

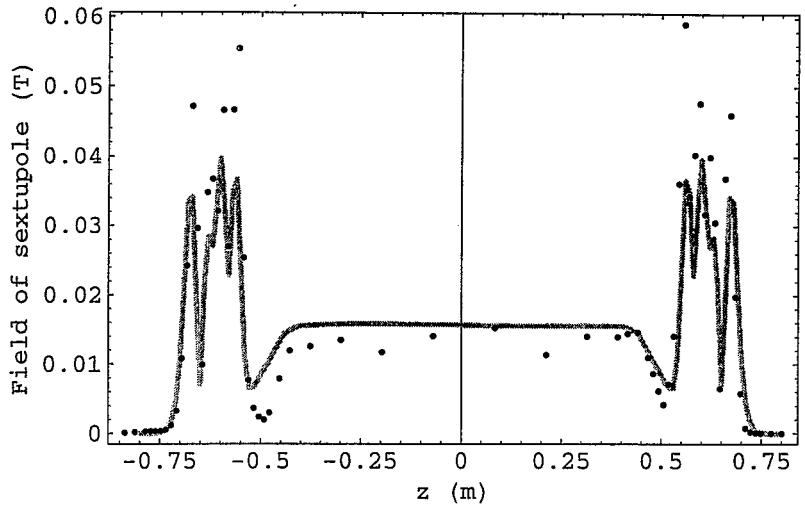

Fig.9. Comparison between measured (dots) and calculated (solid curve) filed intensities of sextupole (n=3) along the beam axis at I = 220 A.

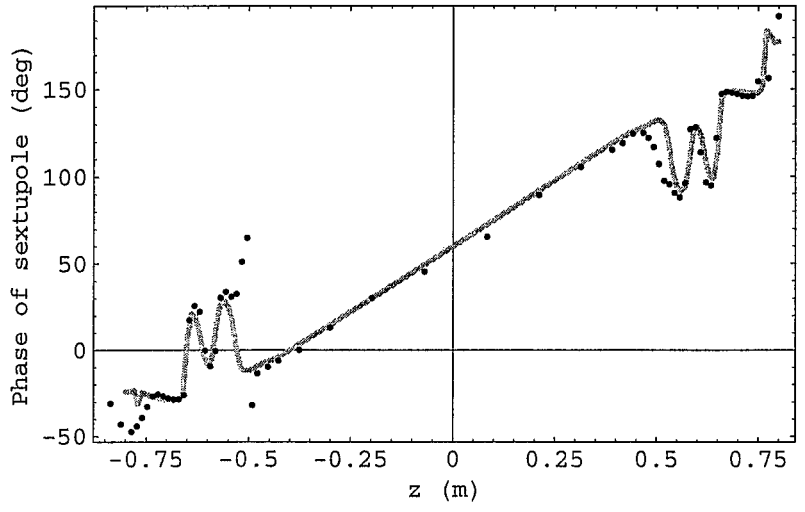

Fig.10. Comparison between measured (dots) and calculated (solid curve) phase angles of sextupole (n=3) along the beam axis at I = 220 A.

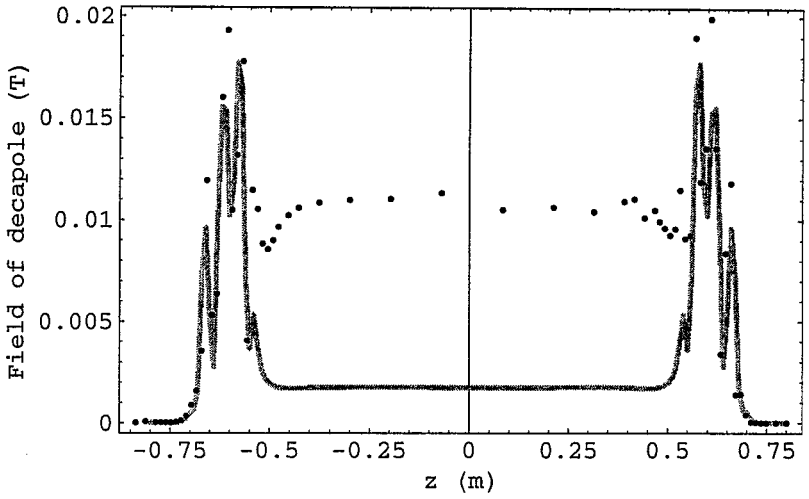

Fig.11. Comparison between measured (dots) and calculated (solid curve) filed intensities of decapole (n=5) along the beam axis at I = 220 A.

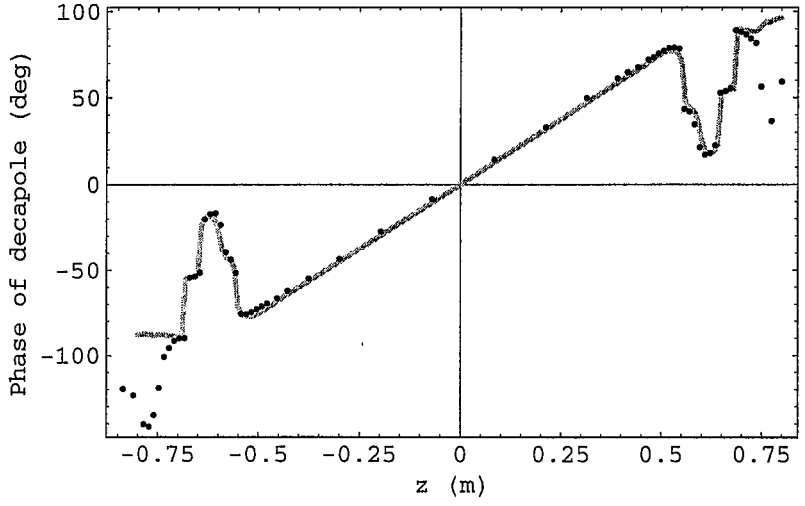

Fig.12. Comparison between measured (dots) and calculated (solid curve) phase angles of decapole (n=5) along the beam axis at I = 220 A.

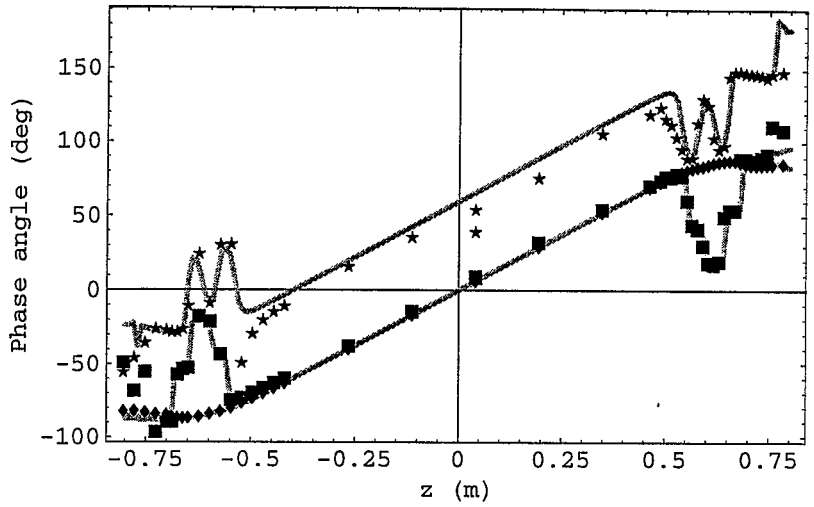

Fig.13. Comparison between measured (dots) and calculated (solid curve) phase angles of dipole (n=1), sextupole (n=3), and decapole (n=5), along the beam axis at I = 105 A.

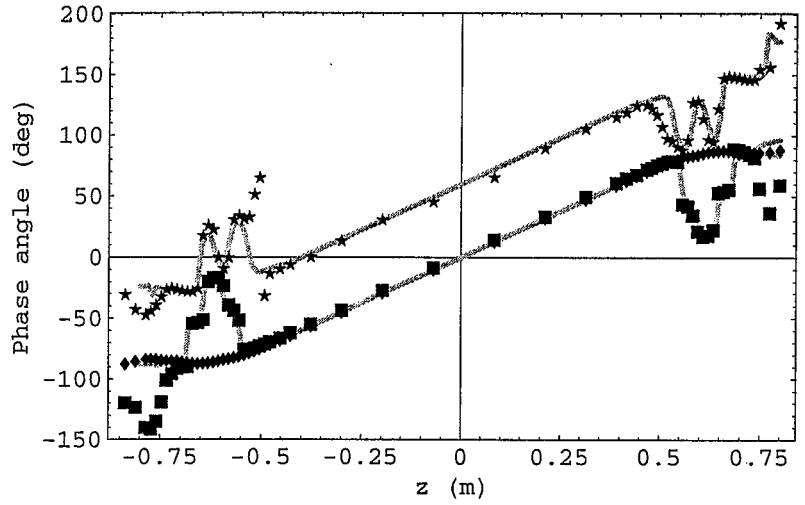

Fig.14. Comparison between measured (dots) and calculated (solid curve) phase angles of dipole (n=1), sextupole (n=3), and decapole (n=5), along the beam axis at I = 220 A.